Spectroscopic Performance of Thick HgI_2 Detectors

L. J. Meng, *Member, IEEE*, Z. He, *Senior Member, IEEE*, B. Alexander, and J. Sandoval

***Abstract*—This paper presents the spectroscopic performance of two newly developed pixelated HgI_2 detectors. These detectors are $1 \times 1 \times 0.814$ cm^3 and $1 \times 1 \times 1.016$ cm^3 in size. Each detector has four closely packed 1×1 mm^2 anode pixels at the center of one of the 1×1 cm^2 surfaces. These anode pixels are surrounded by a large anode. All results presented here are based on events from a sub-volume underneath the anode pixels. In these detectors, signals were read out by a discrete electronics based on multiple A-250 pre-amplifiers and a digital oscilloscope for sampling pulse waveforms. Depth sensing technique was used to correct the depth-dependent variation in photopeak amplitude. Main results presented are: (1) energy resolutions of 0.85 $\sim$ 1.3% have been achieved on these detectors; (2) the electron mobility-lifetime product was measured to be $\sim 1 \times 10^{-2}$ cm^2/V and the measured electron lifetime was ~ 200 μs and (3) variation in electron drifting properties under different anode pixels were observed. Significant non-uniformity in internal electric field strength was also experimentally demonstrated.**

***Index Terms*—HgI_2, Spectroscopic Performance.**

I. Introduction

Hgi_2 is a room temperature semiconductor material with an excellent stopping power and a relatively large photofraction for detecting high energy gamma rays [1]. Due to its wide band gap (2.13 eV), single crystal HgI_2 detectors have a very low leakage current, when compared to other room temperature semiconductor materials, such as Cadmium Zinc Telluride (CZT). However, HgI_2 suffers from relatively low charge carrier mobility and severe material non-uniformity issues. These greatly limit the energy resolution achievable from relatively thick HgI_2 detectors with planar readout anode structures.

To overcome these difficulties, Patt *et al.* proposed and tested HgI_2 detectors that use the single polarity charge sensing technique to reduce the effect of hole trapping in HgI_2 [2]. In their detectors, an anode structure similar to that of silicon drift detectors [3], [4] were fabricated on single crystal HgI_2 materials of 2 mm thick. These devices demonstrated a significantly improved energy resolution. He and Baciak *et al.* used an alternative readout method that is based on finely pixellated anodes [5]. It uses the so-called "small pixel effect" to achieve single polarity charge sensing and reduce the effect of hole trapping. Furthermore, by reading out signals from both anode and cathode simultaneously, one can extract the depth-of-interaction (DOI) for each detected event. This information is then used to correct for the effects of electron trapping and the depth-dependent weighting potential in detector bulk. Energy resolutions of 1.5%–2% at 662 keV have been demonstrated on several $10 \times 10 \times 10$ mm^3 HgI_2 detectors [6], [7]. In this paper, we present a detailed study for evaluating several newly developed HgI_2 detectors having similar configurations.

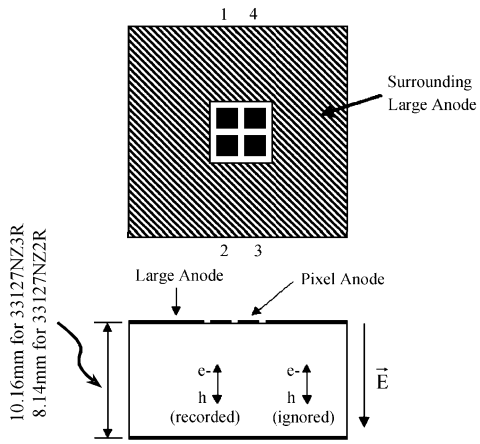

Fig. 1. Configuration of detector 33127NZ2R and 33127NZ3R.

II. Material and Methods

Two HgI_2 detectors tested are $1 \times 1 \times 0.814$ cm^3 (for detector 33127NZ3R) $\sim 1 \times 1 \times 1.016$ cm^3 (for detector #33127NZ2R) in size, with four 1×1 mm^2 anode pixels on one of the 1×1 cm^2 surface surrounded by a large anode. These two detectors will be referred to as Detector #1 and #2 in the following text. The gaps between anode pixels and the large anode are around 150μm wide. A continuous planar cathode was deposited on the opposite side of the crystal. All electrodes are made of palladium. Configurations of these detectors are depicted in Fig. 1. A negative bias voltage was applied to the cathode. All anodes (including the large anode) were DC coupled to multiple A-250 pre-amplifiers [8], while the cathode was AC coupled to another pre-amplifier. Output signals from these preamplifiers were shaped with NIM shaping amplifiers and their outputs were digitized using a digital oscilloscope (HP Infinium). Peak amplitudes were derived by Gaussian fittings to the sampled pulse waveforms. For each detected event, we derived the ratio between signal amplitudes from the cathode and a given anode pixel (which is referred to as C/A in the following text). It was used as a measure of the interaction-depth (measured from the anode plane) in the detector. The depth dependence of anode signal amplitudes can be determined by irradiating the detector with a mono-energetic gamma source and measuring the photopeak position as a function of C/A ratio (as shown in Fig. 2). Once this relationship is established, one can apply a correction factor to each detected event based on the corresponding C/A ratio. This correction ensures that

Manuscript received November 8, 2005; revised March 5, 2006.

L. J. Meng and Z. He are with the Department of Nuclear Engineering and Radiological Sciences, University of Michigan, Ann Arbor, MI 48109 USA (e-mail: ljmeng@umich.edu).

B. Alexander and J. Sandoval are with the Constellation Technology Corporation, Largo, FL 33777 USA.

Digital Object Identifier 10.1109/TNS.2006.873714

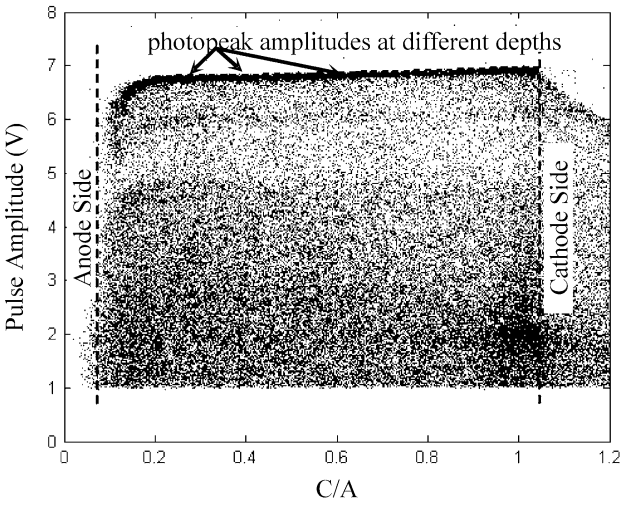

Fig. 2. Anode signal amplitude, measured on Pixel #2 of Detector #1, as a function of the cathode-to-anode ratio (C/A). The detector was biased at -2750 V. A Cs-137 point source was placed on the cathode side of the detector.

the same energy deposition in the detector results in the same mean anode signal amplitude regardless where the energy is deposited. After correction, all events were histogrammed into an energy spectrum and the full-width-at-half-maximum of the (662 keV) photopeak is used as a measure of the energy resolution achieved. Note that for both detectors tested, anode signal amplitudes for the same energy deposition increase with interaction-depth (Fig. 2). As we will show later, these new detectors have an electron lifetime ($\sim 200\mu$s) that is much longer than the actual electron drifting time (<3.2 μs with a bias of $\sim$300 V/mm).

Therefore, the depth-dependence of signal amplitude is dominated by the variation in weighting potential in respect to the anode pixel rather than electron trapping in the material. The latter should cause measured pulse amplitudes decreasing with increasing interaction-depth.

III. Results

A. Spectroscopic Performances

We tested both detectors with a range of cathode biases, ranging from -1750 to -2750 V for Detector #1 and -1500–-3000 V for Detector #2.

Both detectors appeared to be unstable when biased beyond -3000 V. A large fluctuation on pre-amplifier output was observed from the cathode when the breakdown happened. The detectors normally go back to a stable operating condition after lowering the HV. After applying the bias, it takes around seven days for the detectors to settle down. Comparing to Detector #2, Detector #1 requires a higher bias (-1750 versus -1500 V) to become fully depleted although it is 2 mm thinner (8.14 versus 10.16 mm).

Energy resolutions for both detectors were measured using a 10 μCi Cs-137 point source placed close to their cathode sides. We used shaping times of 10 and 16 μs for anode and cathode signals respectively. Fig 3 shows a comparison of Cs-137 energy spectra measured from the four anode pixels on Detector #1. These measurements were taken in April, 2005. The best energy resolution of $\sim 0.9\%$ (5.96 keV) was achieved for all interactions happened across the entire thickness underneath Pixel #2, after correcting for the depth-dependent shift in peak amplitude. For this measurement, the contribution from electronic noise was $\sim$ 2.3 keV measured using a precise pulse generator. With this improved energy resolution, we can now resolve the mercury K α and K β X-ray escape peaks, as shown in Fig. 4. However, a quite large fluctuation in spectroscopic performances across the four pixels was observed (as shown in the first two rows in Table I). The difference in spectroscopic performance, between Pixel #1 and #4, can be visualized by plotting signal amplitude as a function of interaction-depth (as shown in Figs. 2 and 5). For Pixel #4, there is a noticeable blurring around the photopeak that seems to affect all full-energy events regardless their depths-of-interaction. This resulted in an extra broadenings at the low energy side of photopeaks as shown in Fig. 6. This effect was also observed on Pixel #3 of the same detector. For events happened below these pixels, the final charge collection process may be affected by factors such as material defects near these anode pixels or imperfections in pixel fabrication. These may introduce irregular charge loss when electron clouds are drifting close to these pixels and therefore degrade the energy resolution.

When comparing results from two measurements that are 4 months apart, the observed spectroscopic performance of Detector #1 appears changing with time (as shown in Table I). Note that the measured energy resolutions on Pixel #1 and #3 changed noticeably, while the performance of Pixel #2 and #4 were relatively consistent. Over the past 6 month of operation, we did not observe significant polarization on these two detectors.

Within all events detected by Pixels #1 and #2, around 15% are charge sharing events. This fraction was determined by counting the number of events that have >12 keV energy depositions on both Pixel #1 and Pixel #2. In our current detector configuration, there is no steering electrode between anode pixels. As a result, interactions between anode pixels may suffer from charge loss. This effect is evident in Fig. 7, in which we plotted signal amplitudes from anode Pixel #2 against the amplitudes from Pixel #1 (both on Detector #1). Again, a Cs-137 point source was used to irradiate the detector from its cathode side. In this figure, we can see a band of events curved away from the diagonal, which correspond to charge sharing events between the two pixels. The dots on the diagonal are due to events that Compton-scattered under the first pixel and followed by a photoelectric absorption under the second one. For these events, both interactions happened close to the centers of corresponding pixels, they do not suffer severe charge loss under the gap. To quantify the effect of charge loss, we picked a small group of events from a certain depth that having their signal amplitudes on Pixel #1 and #2 (S1 and S2) close to a given ratio. These events are likely to be from a given lateral position between two pixels. We derived the centroid of these dots and the amount of charge loss was estimated as shown in Fig. 7. This process was repeated for several given depths and the results are summarized in Table II. It is not surprised that charge loss is the most significant ($>15\%$) for events at the center between the two pixels ($S1 \approx S2$) and close to the anode

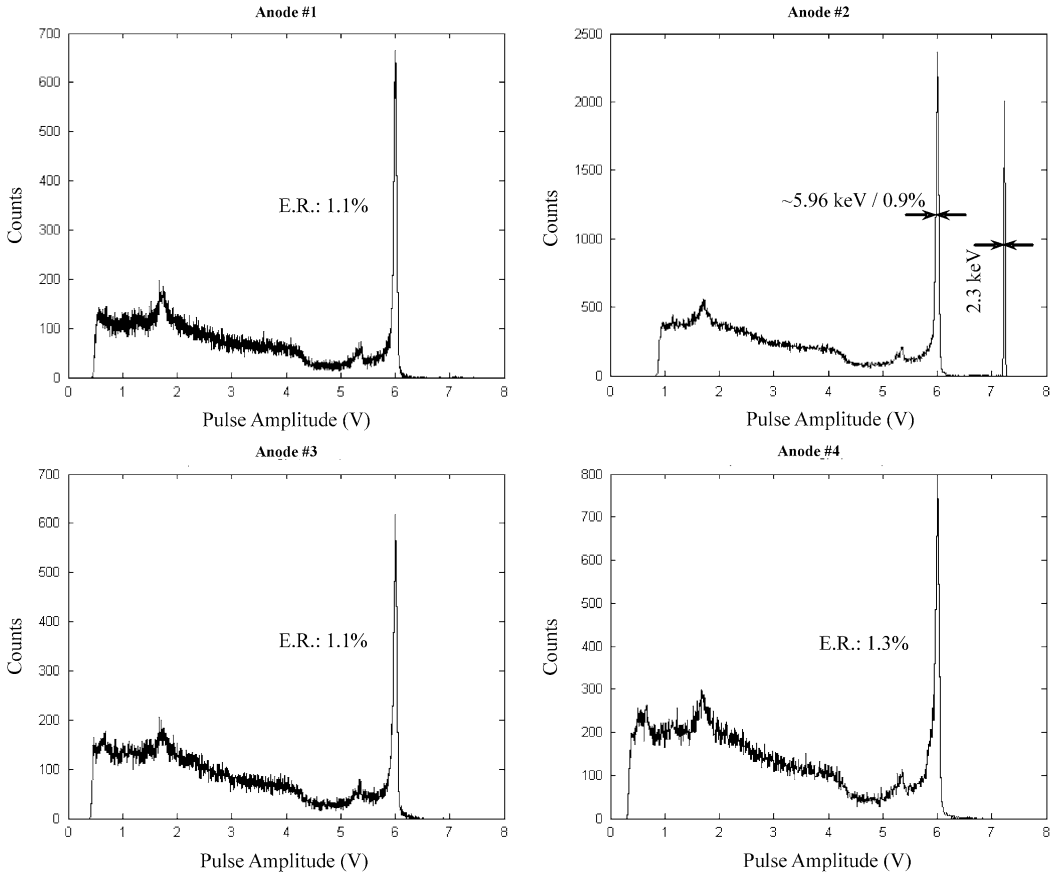

Fig. 3. Energy resolutions measured from the four anode pixels on Detector #1. The detector was biased at -2750 V. Measurements were taken at April 20-24, 2005.

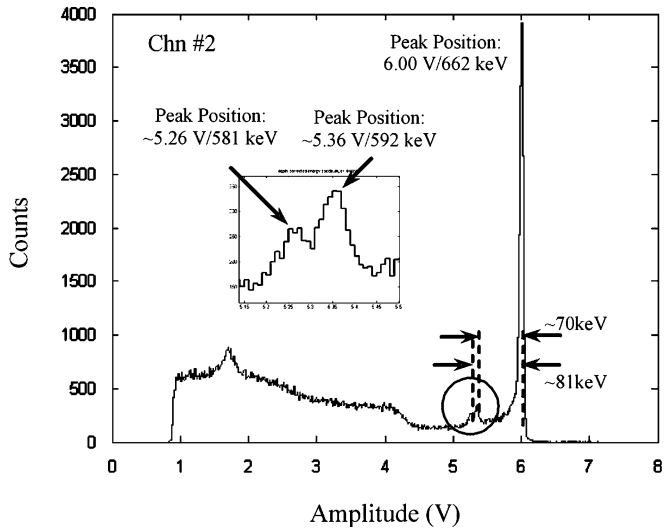

Fig. 4. Mercury K α and K β X-ray escape lines measured on Pixel #2 of Detector #1.

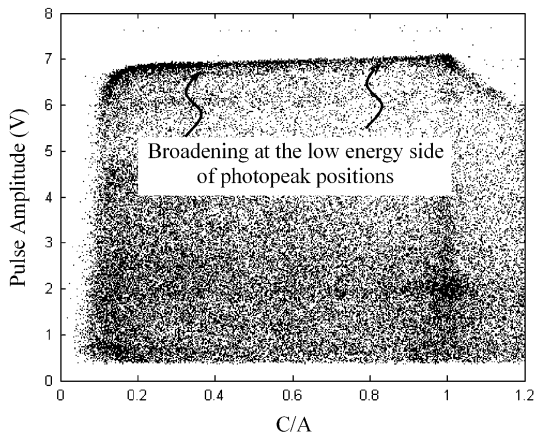

Fig. 5. Anode signal amplitude as a function of the cathode-to-anode ratio (C/A) measured on Pixel #4, Detector #1. The detector was biased at -2750 V. A Cs-137 point source was placed on the cathode side of the detector.

plane. It decreases gradually when events are shifting towards one pixel (S1/S2 moving towards 8) and occurring deeper in the detector. A measured energy spectrum for charge sharing events is shown in Fig. 8. These charge loss events caused extra spreading of the photopeak towards its lower energy side. They also added heavy tailing between the photopeak and the Compton edge. The effect of charge sharing can be reduced by using larger anode pixels and reducing the width of the gap between pixels.

B. Electron Mobility and Lifetime Measurements

The mobility-lifetime product for electrons was experimentally measured using the method described in [9]. By varying detector bias, the amount of electron trapped in the detector

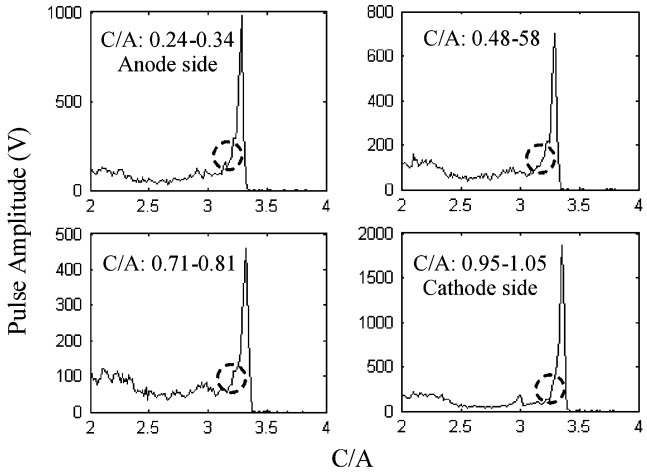

Fig. 6. Measured energy spectra with events from different interaction depths. Data was taken from Pixel #4 on Detector #1. The tailing effects at the low energy side of photopeaks are marked by dashed circles.

TABLE I
MEASURED ENERGY RESOLUTIONS

Measurements	Pixel #1	Pixel #2	Pixel #3	Pixel #4
Det #1 April, 2005 -2750V	1.1% (0.5%)*	0.90% (0.4%)	1.0% (0.4%)	1.3% (0.4%)
Det #1 Sept., 2005 -2750V	0.8% (0.4%)	0.9% (0.4%)	1.3% (0.4%)	1.3% (0.4%)
Det #1 Sept., 2005 -1750V	1.6%	2.0%	2.2%	1.9%
Det #2 April, 2005 -3000V	1.6% (0.63%)	1.5% (49%)	1.7% (0.48%)	--
Det #2 April, 2005 -2250V	1.4%	1.3%	1.9%	--
Det #2 April, 2005 -1500V	3.8%	1.8%	2.1%	--

* Measured electronic noise contribution.

varies due to the difference in electron drifting time. We used an Am-241 point source placed close to the cathode side to ensure that all electrons are drifting through the silimar distance regardless what bias is applied. $(\mu\tau)_e$ can be derived using the following equation:

$$(\mu\tau)_e = \frac{z \cdot D}{\ln(A_1/A_2)} \left(\frac{1}{V_2} - \frac{1}{V_1}\right)$$

where A_1 and A_2 are photopeak positions for cathode-side events measured at two different bias, V_1 and V_2, respectively. D is the thickness of the detector. In these measurements, all experimental conditions are kept the same except the bias voltage applied. The accuracy for estimating $(\mu\tau)_e$ is affected by uncertainties on the estimated detector thickness D, the

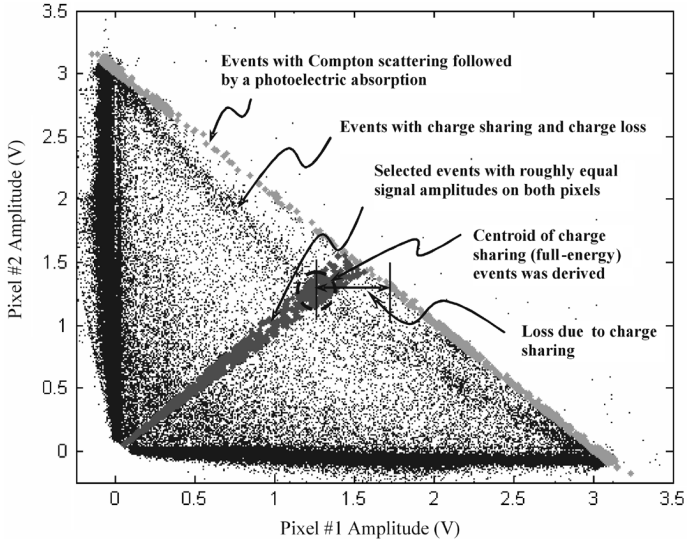

Fig. 7. Pixel #2 signal amplitude versus Pixel #1 amplitude. Data was taken in April, 2005 with Detector #1, biased at -2750 V.

TABLE II
CHARGE LOSS AT DIFFERENT INTERACTION DEPTHS AND CHARGE SHARING CONFIGURATIONS

S1/S2	C/A=5	C/A=10	C/A=15	C/A=20
1	15.8%	14.8%	14.4%	13.3%
2	14.5%	13.2%	12.4%	12.3%
4	10.5%	10.1%	10.0%	9.2%
8	7.9%	6.2%	6.1%	5.4%

electrons drifting length z and the measured photopeak positions V_1 and V_2. It can be approximated using the standard error propagation formula

$$\frac{\sigma^2[(\mu\tau)_e]}{[(\mu\tau)_e]^2} \approx \frac{\sigma^2(z)}{z^2} + \frac{\sigma^2(D)}{D^2} + \left[\frac{1}{\ln(A_1/A_2)}\right]^2 \cdot \left[\frac{\sigma^2(A_1)}{A_1^2} + \frac{\sigma^2(A_2)}{A_2^2}\right] + \left[\frac{z \cdot D}{\ln(A_1/A_2)}\right]^2 \cdot \left[\frac{\sigma^2(V_1)}{V_1^2} + \frac{\sigma^2(V_2)}{V_2^2}\right].$$

We used Gaussian fitting to find photopeak positions. The fitting process also returned standard deviations associated with estimated peakpositions. For this measurement, $\sigma(A_1)/A_1$ and $\sigma(A_2)/A_2$ were both less than 0.03%. So their contributions to the overall error are negligible compared with other factors. We also assumed that errors on the bias voltages applied (V_1 and V_2) and the detector thickness D are negligible. Therefore, the single greatest error source is the error on the estimation of electron drifting distance z. 59 keV gamma rays emitted by the Am-241 source has an attenuation length of ~ 170 μm in HgI_2. The exponential distribution of interaction sites has a standard deviation of 170 μm. From these, we get

$$\frac{\sigma[(\mu\tau)_e]}{[(\mu\tau)_e]} \approx \frac{\sigma(z)}{z} = \frac{0.17\ (\text{mm})}{10.16\ (\text{mm}) - 0.17\ (\text{mm})} = 1.7\%.$$

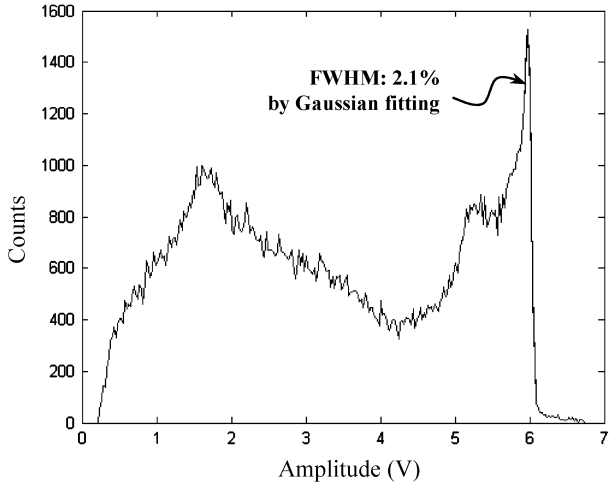

Fig. 8. Measured energy spectrum using events that having greater than 12 keV signals on both Pixel #1 and Pixel #2. Data was taken in September 2005 with Detector #1, biased at -2750 V.

TABLE III
MEASURED $(\mu\tau)_e$ FOR DETECTOR #1

	Pixel #1	Pixel #2	Pixel #3	Average
$(\mu\tau)_e$ (cm^2/V)	1.0×10^{-2}	1.3×10^{-2}	1.2×10^{-2}	1.2×10^{-2}
τ_e (μs)	210	220	200	210
μ_e ($cm^2/V\cdot s$)	50	60	61	57

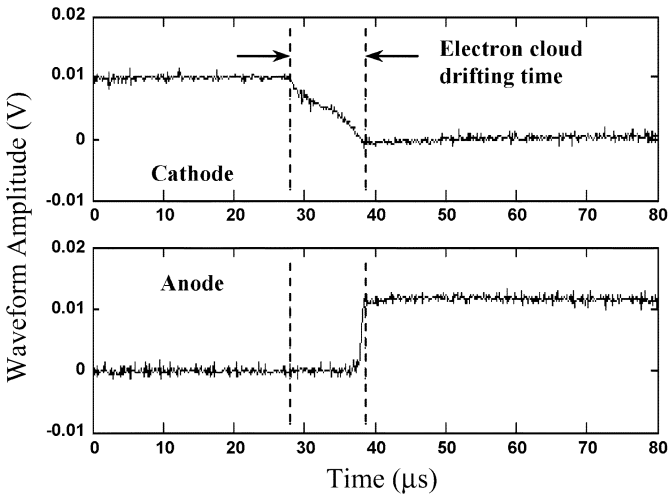

Fig. 9. Measuring electron cloud drifting time

The measured $(\mu\tau)_e$ values for several anode pixels are shown in Table III.

In this study, we also measured electron lifetime in these detector. The time taken by electrons to drift through the entire detector thickness can be accurately determined using pulse waveform analysis [10], [11]. A typical cathode pulse waveform is shown in Fig. 9, along with the corresponding pre-amplifier waveform from the anode pixel. The turning points in the cathode waveform can be used as the starting and ending times for a given electron drifting period. At a given bias voltage, we picked a number of cathode-side events and derived an average drifting time. For this measurement, we used a Cs-137 point source (instead of an Am-241 source) to irradiate the detector from its cathode side, because electron drifting time can be measured with better precision at higher energy. Electron lifetime can be derived using the following equation [12]:

$$\tau_e = \frac{t_2 - t_1}{\ln(A_1/A_2)}$$

where t_1 and t_2 are average electron drifting times at two different biases. A_1 and A_2 are the corresponding photopeak positions. In this method, the major source of error is the uncertainty on estimated electron drifting times. The average electron drifting times for cathode-side events under Pixel #2 on Detector #2 were 10.5 ± 0.58 μs at -3000 V and 4.9 ± 0.24 μs at -1500 V. Therefore the relative error is given as

$$\frac{\sigma(\tau_e)}{\tau_e} \approx \sqrt{\frac{\sigma^2(t_2) + \sigma^2(t_1)}{(t_2 - t_1)^2}} = \sqrt{\frac{(0.58\,\mu s)^2 + (0.24\,\mu s)^2}{(5.6\,\mu s)^2}} = 11.2\%.$$

Although similar ($(\mu\tau)_e$ values have recently been reported for CZT detectors measured with similar techniques[13], the actual electron drifting characteristics are quite different in CZT and HgI_2. In HgI_2, electrons drift more than an order of magnitude slower than in CZT. Fortunately, the very long electron lifetime in HgI_2 compensates for the slow carrier movement. As long as the shaping time used is sufficiently long, a very high charge collection efficiency can be achieved. Note that the measured $(\mu\tau)_e$ shown in Table III are higher than those previously reported by Baciak *et al.* [6], [7], Bolotnikov *et al.* [14], and Hitomi *et al.* [15]. Improvement in material quality, especially in electron drifting characteristics may be the key for the dramatic improvements in spectroscopic performance of thick HgI_2 detectors.

C. Mean Cathode Waveforms

In order to gain extra information on electron drifting behavior, cathode pre-amplifier pulse waveforms were recorded for each detected event. We selected full-energy, cathode-side events underneath a given anode pixel and derived a mean cathode waveform for this group of events. A comparison between mean waveforms for the four anode pixels on Detector #1 is shown in Fig. 10. One can see clear differences between waveforms corresponding to different anode pixels. Note that the standard deviations on these mean waveforms are experimentally determined to be less than 3×10^{-5}V, which is negligible when compared to the scale of these differences. When the detector was biased at -2750 V, electron clouds generated under Pixel #4 tend to drift for longer before getting collected. Another interesting feature is the bending on these waveforms. The slopes of mean waveforms are shown in Fig. 11. If one assumes that all electrons are traveling on straight lines perpendicular to the cathode plane and the electron mobility is constant, the slope of mean cathode waveforms should

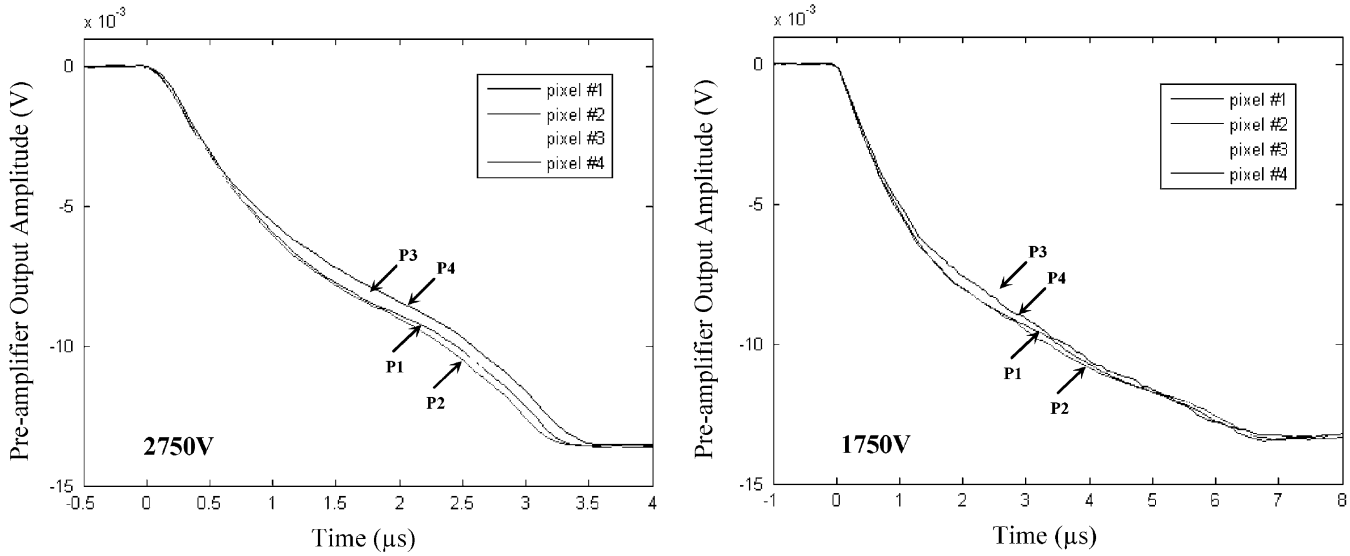

Fig. 10. Comparing mean pre-amplifier waveforms for interactions occur near the cathode and beneath anode Pixel #1-4. Data taken in September 2005 with Detector #1. Two different biases were used.

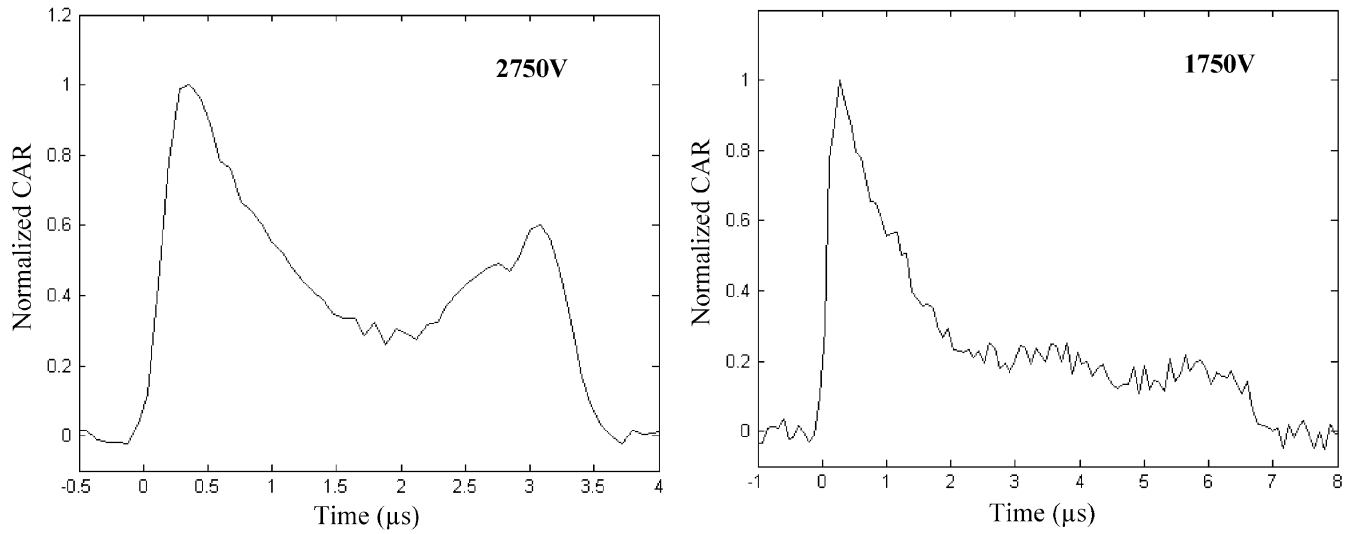

Fig. 11. Normalized CAR curves for Detector #1 biased at -1750 and -2750 V. Data taken in September 2005.

be proportional to electric field strength inside the detector. When the detector was biased at -2750 V, the slope changed by a factor of 3 from cathode side to anode side. The highest electric field strength was formed close to the cathode surface. An even greater variation was observed when the detector was biased at -1750 V. Such effect was also observed on several other HgI_2 detectors tested.

IV. Conclusion

In this paper, we reported detailed evaluations of two thick HgI_2 detectors. Some key results from this study are summarized as the following.

- Below 1% energy resolution at 662 keV was measured from several pixels on Detector #1.
- Pixel-to-pixel variation in energy resolution was observed on both detectors. The poor energy resolution from certain anode pixels may be due to crystal defect near the anode pixels or imperfection on pixel fabrication.
- Due to the lack of steering electrode between anode pixels, charge loss was significant for events between anode pixels. This effect greatly degrades the spectroscopic performance of the detector when including these charge sharing events.
- The measured electron mobility-lifetime product was $\sim 1 \sim 1 \times 10^{-2}$ (cm^2/V) for these detectors. Electron lifetime in Detector #2 was measured to be ~ 200 μs.
- In these detectors, we observed severe variation in internal electric field strength from cathode to anode sides. This seems to be a common feature amongst several other HgI_2 detectors that we have evaluated.
- Energy resolution of these detectors changed with time. Over the past six month period after applying the bias, we did not observe severe polarization effect.

- After initial biasing, these detectors normally require at least 7 days to settle down.

With current fabrication process, it is difficult to deposit very fine steering electrodes between anode pixels. Detectors with more anode pixels of various sizes will be tested, which should provide more insights into the effect of charge sharing on spectroscopic performance of these thick HgI_2 detectors. Fully pixilated HgI_2 detectors using ASIC readout are under development.

REFERENCES

[1] W. R. Willig, "Mercury iodide as a gamma spectrometer," *Nucl. Instrum. Meth.*, vol. 96, p. 615, 1971.

[2] B. E. Patt, J. S. Iwanczyk, G. Vilkelis, and Y. J. Wang, "New gamma-ray detector structures for electron only charge carrier collection utilizing high-z compound semiconductors," *Nucl. Instrum. Meth. Phys. Res. A*, vol. 380, pp. 276–281, 1996.

[3] E. Gatti, P. Rehak, and J. T. Walton, "Silicon drift chambers—1st results and optimum processing of signals," *Nucl. Instrum. Meth. Phys. Res. A*, vol. 226, pp. 129–141, 1984.

[4] C. Fiorini, F. Perotti, and C. Labanti, "Performances of a silicon drift chamber as fast scintillator photodetector for gamma-ray spectroscopy," *IEEE Trans. Nucl. Sci.*, vol. 45, no. 3, pp. 483–486, Jun. 1998.

[5] Z. He and R. D. Vigil, "Investigation of pixellated HgI2 gamma-ray spectrometers," *Nucl. Instrum. Meth. Phys. Res. A*, vol. 492, pp. 387–401, 2002.

[6] J. E. Baciak and Z. He, "Comparison of 5 and 10 mm thick HgI2 pixelated gamma-ray spectrometers," *Nucl. Instrum. Meth. Phys. Res. A*, vol. 505, pp. 191–194, 2003.

[7] J. E. Baciak and Z. He, "Spectroscopy on thick HgI2 detectors: A comparison between planar and pixelated electrodes," *IEEE Trans. Nucl. Sci.*, vol. 50, no. 4, pp. 1220–1224, Aug. 2003.

[8] *A-250 Product Datasheet*, [Online]. Available: http://www.amptek.com/a250.html.

[9] Z. He, G. F. Knoll, and D. K. Wehe, "Direct measurement of product of the electron mobility and mean free drift time of CdZnTe semiconductors using position sensitive single polarity charge sensing detectors," *J. Appl. Phys.*, vol. 84, pp. 5566–5569, 1998.

[10] L. J. Meng and Z. He, "Estimate interaction timing in a large volume HgI_2 detector using cathode pulse waveforms," *Nucl. Instrum. Meth. Phys. Res. A*, vol. 545, pp. 234–251, 2005.

[11] L. J. Meng and Z. He, "Exploring the limiting timing resolution for large volume CZT detectors with waveform analysis," *Nucl. Instrum. Meth. Phys. Res. A*, vol. 550, pp. 435–445, 2005.

[12] Z. He, G. F. Knoll, and D. K. Wehe, "Direct measurement of electron drift parameters of wide band gap semiconductors," *Nucl. Instrum. Meth. Phys. Res. A*, vol. 411, pp. 114–120, 1998.

[13] F. Zhang, Z. He, D. Xu, G. F. Knoll, D. K. Wehe, and J. E. Berry, "Improved resolution for 3-d position sensitive CdZnTe spectrometers," *IEEE Trans. Nucl. Sci.*, vol. 51, no. 5, pp. 2427–2431, Oct. 2004.

[14] A. E. Bolotnikov, J. Baker, R. DeVito, J. Sandoval, and L. Szurbart, "HgI2 detector with a virtual Frisch ring," *IEEE Trans. Nucl. Sci.*, vol. 52, no. 1, pp. 468–472, Feb. 2005.

[15] K. Hitomi, L. J. Meng, and Z. He, "Evaluation of pixellated HgI_2 detectors," presented at the IEEE NSS/MIC Conf. Rec., Rome, Italy, 2004.